Energy & Environmental Science

COMMUNICATION

View Article Online
View Journal | View Issue

Effective nonmetal incorporation in black titania with enhanced solar energy utilization†

Cite this: *Energy Environ. Sci.*, 2014, **7**, 967

Received 9th August 2013
Accepted 19th November 2013

DOI: 10.1039/c3ee42708k

www.rsc.org/ees

Tianquan Lin,[a] Chongyin Yang,[a] Zhou Wang,[a] Hao Yin,[a] Xujie Lü,[a] Fuqiang Huang,*[ab] Jianhua Lin,[b] Xiaoming Xie[c] and Mianheng Jiang[c]

Nonmetal-doped black titania is achieved in a core–shell structure by a two-step synthesis. The nonmetal dopants in amorphous TiO_{2-x} shells decrease e–h recombination centers, and more than 6.6 at.% N further improves solar energy absorption from 65% up to 85%. The photocatalytic H_2 generation of the N-doped black titania is 15.0 mmol h^{-1} g^{-1} under 100 mW cm^{-2} of full-sunlight and 200 μmol h^{-1} g^{-1} under 90 mW cm^{-2} of visible-light irradiation, superior to TiO_{2-x} and reported titania photocatalysis.

Titanium dioxide (TiO_2) as a wide bandgap semiconductor has been a well-known photocatalyst since the first demonstration of water splitting over TiO_2 by Fujishima and Honda in 1972.[1–3] Over the past 40 years, research on visible-light photoactive titania has been focused on metal and nonmetal-ion substitution.[4–9] Nonmetal X doping (X = N, ~6–12.5 at.% from theoretical simulations) were predicted to contribute to the extension of the light absorption wavelength range.[4,7,10] Many experimental results confirmed that the incorporation of X (X = B, N, C, S) improved visible-light photocatalysis compared with pristine titania, but the visible light absorption was not significantly enhanced probably due to a low lattice doping level of X.[11,12] However, the limited solubility of substitutional dopants in bulk and dopant associated recombination centres has impaired the effectiveness of doping.[13] Therefore, heavy nonmetal doping into titania, which benefits wide-spectrum solar absorption and efficient power conversion, is still a big synthesis issue.

Very recently, black coloration of TiO_2 was prepared by generating oxygen vacancies from hydrogen reduction,[14–18] as well as other reduction methods (Al, Zn, *etc.*)[19] or some oxidation method (TiH_2, *etc.*).[20] Most black titania boosted visible light absorption[16,17,19–24] but was unsatisfactory in improving visible-light photocatalysis,[5,14,25–28] which was attributed to the short lifetime of light-excited electrons and holes.[29] These oxygen vacancies were reported to cause trapped states in the forbidden bandgap, 0.75–1.18 eV away from the conduction band minimum.[30–32] Excessive oxygen vacancies can become e–h recombination centers and harm its photocatalysis.

In this research, nonmetal atoms are proposed to reduce oxygen vacancies in black TiO_{2-x}. A novel two-step approach is illustrated in Scheme 1 to prepare nonmetal-doped black titania. Many oxygen vacancies are first introduced in TiO_2

Broader context

The important semiconductor TiO_2 has found applications in a wide range of technological innovations. When used as a photocatalyst, TiO_2 absorbs only ultraviolet light. Several approaches, including the use of dopants or introducing disorder in the surface layers of TiO_2 colored in black, have been taken to enhance the visible light absorption. However, the limited solubility of substitutional dopants in bulk and dopant associated recombination centres (*i.e.* Ti^{3+}) has impaired the effectiveness of doping. In addition, for black titania, the visible-light photocatalytic activity is still unsatisfactory due to too many recombination centers. To overcome this bottleneck, we demonstrate a novel two-step approach to enhance the visible-light photocatalytic activity by incorporating nonmetal X (X = H, N, S, I) into oxygen-deficient titania (TiO_{2-x}). The bulk substitutional doping of titania with 6.6 at.% nitrogen (TiO_2–N) absorbs about 85% of the total solar energy and exhibits substantial visible-light photocatalytic activity, including the complete photo-oxidation of organic molecules in water within 6 min and the production of hydrogen (15.0 mmol h^{-1} g^{-1} under full-sunlight and 200 μmol h^{-1} g^{-1} under visible light). The excellent photocatalysis of TiO_2–X is attributed to visible-light absorption enhancement and recombination center reduction.

[a]*State Key Laboratory of High Performance Ceramics and Superfine Microstructure and CAS Key Laboratory of Materials for Energy Conversion, Shanghai Institute of Ceramics, Chinese Academy of Sciences, Shanghai 200050, China. E-mail: huangfq@mail.sic.ac.cn*

[b]*College of Chemistry and Molecular Engineering, Peking University, Beijing 100871, China*

[c]*State Key Laboratory of Functional Materials for Informatics, Shanghai Institute of Microsystem and Information Technology, Chinese Academy of Sciences, Shanghai 200050, P. R. China*

† Electronic supplementary information (ESI) available: The equipment schematics for preparation of TiO_2–X; preparation of X-doped TiO_2 following the literature methods and their photocatalysis; elemental abundances; HRTEM images, XRD patterns, XPS VB spectra, and magnetic field dependence of magnetization of TiO_2–X. See DOI: 10.1039/c3ee42708k

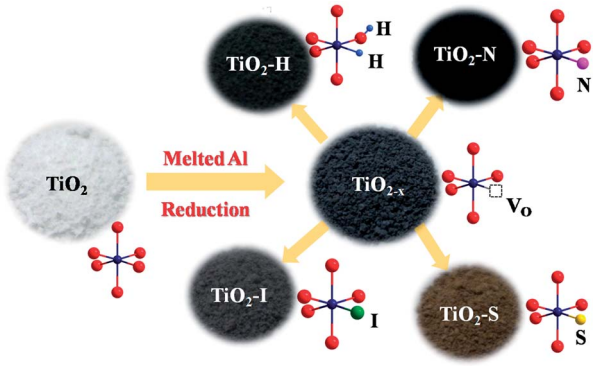

Scheme 1 Schematic evolution from pristine TiO_2 to oxygen-deficient titania (TiO_{2-x}) and then to X-doped titania (TiO_2–X; X = H, N, S, I).

(Degussa P25) nanocrystals by the reduction of molten Al in an evacuated two-zone furnace according to our previous work.[28] The experimental setup and formation mechanism of TiO_{2-x} are provided in the ESI.† The oxygen-deficient amorphous layers of Al-reduced titania nanocrystals (TiO_{2-x}) are ready to accept nonmetal incorporation of X (X = H, N, S, I). From this synthesis strategy, more X atoms are expected to be filled in oxygen vacancies in black titania.

The oxygen-deficient titania nanocrystals (TiO_{2-x}, ~25 nm in diameter) contain an amorphous surface layer surrounding the crystalline TiO_2 core confirmed by high-resolution transmission electron microscopy (HRTEM), as shown in Fig. 1. The average thickness of the amorphous layers (~4 nm) is thicker than the reported TiO_{2-x} directly reduced by H_2 gas.[14] It indicates that more efficient reduction can be achieved in our Al-reduced sample than the H_2-reduced samples, consistent with the Ellingham diagram shown in Fig. S1 of the ESI.† The amorphous shell in the Al-reduced sample loses lattice ordering with many oxygen vacancies (or say, Ti^{3+} ions). The oxygen vacancies are beneficial for the X atoms diffusing into the amorphous shell and occupy these oxygen vacancies, illustrated in Fig. 1a. The conversion from Ti^{4+} into Ti^{3+} arises as some electrons are occupied in the Ti^{4+} $3d^0$ states and result in the Ti^{3+} $3d^1$ states in the conduction band.[6] The disordered shell retains a similar thickness after the nonmetal incorporation (Fig. S4†). The TEM results demonstrate that the crystal size of black TiO_{2-x} does not increase obviously after the Al reduction, further confirmed by similar BET specific surface areas for these black TiO_{2-x} (~42 m^2 g^{-1}) and pristine TiO_2 (~43 m^2 g^{-1}). In contrast, these reported nonmetal doped TiO_{2-x} samples were prepared from a one-step reaction of crystalline TiO_2 and X-containing precursor, which is much more difficult for X atoms to enter the TiO_2 lattice. The underlying reasons include that the diffusion rate of X is much lower in crystalline TiO_2 than in amorphous TiO_{2-x}, furthermore less electronegative X atoms are harder to replace the O atoms with. The energy dispersive spectra (Fig. S5†) of nonmetal doped TiO_2 from TEM measurements confirm the existence of nonmetal elements in the nonmetal-doped black titania. The strong diffraction peaks in the X-ray power diffraction patterns (Fig. S6†) indicate that pristine TiO_2, black TiO_{2-x} and nonmetal-doped TiO_2–X retain high crystallinity. Nevertheless, the black TiO_{2-x} exhibits a larger peak width than pristine TiO_2, derived from oxygen vacancies and the resulting disorder-induced lattice strain.

As the unique crystalline-disordered core–shell structure was formed, the TiO_{2-x} sample was colorized black. Compared with pristine and the reported black titania (obtained by H_2 reduction), our TiO_{2-x} sample significantly enhanced the absorption of visible and near infrared light as shown in Fig. 1c and S9.† After the X (H, N, S, I) atoms were introduced into the TiO_{2-x}, the absorption spectra reveal a further enhancement in Fig. 1c. For example, the N-doped black titania (TiO_2–N) possesses far larger solar absorption (~85% of solar spectral irradiance, the calculation details are described in the ESI†) than TiO_{2-x} (~65%) and the reported black titania (<30%). The absorption edge of TiO_2–X near 400 nm from the core of crystalline TiO_2 corresponds to ~3.2 eV. The secondary absorption edge due to the additional valence states from doped nonmental atoms were observed in TiO_2–N (2.5 eV) and TiO_2–S (1.9 eV). These results agree well with the XPS valence band shown in Fig. S10.† Following literature preparations,[4,33] the as-synthesized N- and S-doped TiO_2 also possess some visible-light absorption, but their absorptions do not cover a spectral range as wide as the TiO_2–X, as shown in Fig. S9.†

The X atoms chemically bonding with Ti and elemental contents were observed in the X-ray photoelectron spectroscopy (XPS) measurements, as shown in Fig. 2. The N 1s XPS peak (Fig. 2a) at 396.3 eV and 399.8 eV obtained from TiO_2–N are assigned to Ti–N bonding due to the substitutional N dopants and Ti–O–N due to the interstitial N, respectively.[7,34] Their ratio is ~5 : 1 according to the area ratio of N 1s peaks. The tail in the N 1s peak at 397.7 eV was derived from absorbed oxygen forming the Ti–N–O band.[35] The N incorporation was further confirmed by Ti 2p XPS in Fig. 2b. The binding energies of 456.3 eV ($2p_{3/2}$) and 462.8 eV ($2p_{1/2}$) are associated with the configuration of the TiN phase corresponding to substitutional N,[36] and the peak at 457.8 eV ($2p_{3/2}$) is due to the formation of Ti–O–N

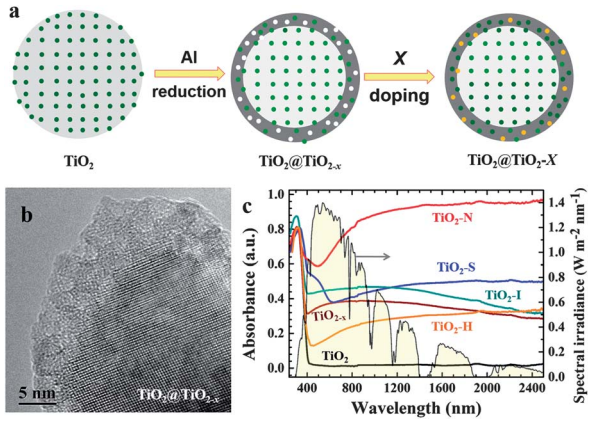

Fig. 1 (a) Schematic core–shell structures of TiO_2@TiO_{2-x} (denoted as TiO_{2-x}) and TiO_2@TiO_2–X (denoted as TiO_2–X) with the Ti^{4+}, oxygen vacancies and X sites in green, white and orange, respectively. (b) HRTEM image of black TiO_{2-x} nanocrystal. (c) Diffuse reflectance spectra of TiO_2–X (X = H, N, S, I) and solar spectral irradiance (right).

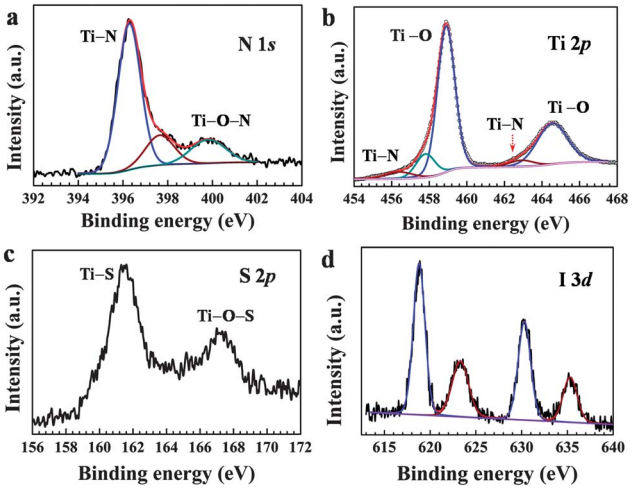

Fig. 2 (a and b) High resolution XPS spectra of N 1s and Ti 2p of TiO_2–N, (c) S 2p XPS spectrum of TiO_2–S, (d) I 3d XPS spectrum acquired from TiO_2–I.

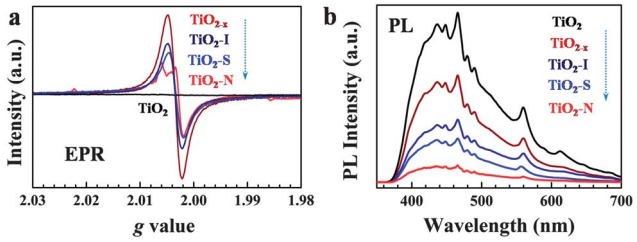

Fig. 3 (a) EPR spectra and (b) PL spectra of TiO_{2-x}, TiO_2–I, TiO_2–N, TiO_2–S and pristine TiO_2.

bond.[37] Two XPS peaks of S 2p were observed at around 161.6 and 167.4 eV in the TiO_2–S as shown in Fig. 2c. They were assigned to Ti–S and Ti–O–S bonding ascribed to substitutional and interstitial S dopants, respectively.[38,39] The XPS spectra of the I 3d show two doublet peaks at 623.3 (I $3d_{5/2}$) and 635.2 eV (I $3d_{3/2}$) and at 618.8 (I $3d_{5/2}$) and 630.6 (I $3d_{3/2}$) eV, respectively, suggesting that I exists with multi-valency in the TiO_2–I sample.[40–42] Our XPS analysis determined that the nonmetal (N, S, I) contents were 6.62 at.% for TiO_2–N, 5.12 at % for TiO_2–S and 4.31 at % for TiO_2–I (Table S1†). The doping level is higher than the reported nonmetal doped titania.[4,7,40–42] These results indicate the oxygen vacancies in TiO_{2-x} were partially filled by the nonmetal X atoms. Moreover, no aluminum signal between 72 and 75 eV was detected in the XPS full-scale spectra of TiO_2–X shown in Fig. S7.†

The incorporation of X (H, N, S, I) into the shell of TiO_{2-x} can modify the electronic structure by converting Ti^{3+} into Ti^{4+} and filling oxygen vacancies (reducing some dangling bonds), which are favorable for improving visible light absorption and efficient carriers (hole) migration. The valence orbitals of X at the valence band maximum are more delocalized than the O 2p due to lower electronegativity and higher polarizability. In contrast, some d-block metal doping often generates deeply localized d states in the forbidden band gap of TiO_2 and results in recombination centers for carriers.[4] The electron paramagnetic resonance (EPR) and magnetic field dependence of the magnetization results recorded at 300 K clearly show the surface oxygen vacancies or unpaired spins of Ti^{3+} $3d^1$ in the samples. Fig. 3a shows the EPR results of the pristine TiO_2, TiO_{2-x} and TiO_2–X. The *g*-value is 2.003 for TiO_{2-x} and TiO_2–X, corresponding to unpaired electrons trapped by oxygen vacancies.[43,44] The EPR intensities reduced when these X atoms were introduced in the TiO_{2-x} confirming that the content of oxygen vacancies decreases after X atom incorporation. The spectrum of TiO_2–N is composed by two overlapped signals respectively due to O_2^- and NO^{2-}, similar to previous reports.[45,46] The magnetic field dependence of magnetization demonstrates reduction of the content of Ti^{3+} after X incorporation due to weaker ferromagnetism correlating with a lower concentration of unpaired spins from Ti^{3+}, as shown in Fig. S11.†

The photoluminescence (PL) spectra are useful to understand the behavior of light-generated electrons and holes in photocatalysts since PL emission results from the recombination of electrons and holes.[47,48] The PL spectra of titania samples in the wavelength range of 350–700 nm with excitation at 320 nm are shown in Fig. 3b. The PL intensities of the TiO_2–X decrease compared with TiO_2. The downward trend of these black titania is TiO_2–N < TiO_2–S < TiO_2–I < TiO_{2-x}, consistent with the results of EPR and magnetism. The recombination of electrons and holes in TiO_2–X significantly decreases, which benefits the photocatalysis.

The excellent photocatalytic activities of the TiO_2–X samples were first demonstrated by H_2 generation, as illustrated in Fig. 4 and listed in Table 1. The hydrogen generation of Al-reduced TiO_{2-x} (6.2 mmol h^{-1} g^{-1}) under the full-sunlight irradiation is eight times higher than pristine TiO_2 (0.75 mmol h^{-1} g^{-1}). It is noteworthy that the TiO_2–N steadily produced H_2 gas at 15.0 mmol h^{-1} g^{-1}, which belongs to the best ranks (~10 mmol h^{-1} g^{-1}) in semiconductors for photogenerating H_2.[49–51] The H_2 generation of TiO_2–S and TiO_2–I are 12.1 mmol h^{-1} g^{-1} and 10.3 mmol h^{-1} g^{-1}, respectively, also superior to that of reported black TiO_{2-x}.[50] We also measured photocatalytic H_2 generation using TiO_2–X as the photocatalyst with only visible and infrared light by cutting off the UV light shorter than about 400 nm. The enhancement of the TiO_2–X under the visible-light irradiation is apparently shown in Fig. 4b. Again, the visible-light H_2 generation of all the TiO_2–X samples are more efficient than TiO_{2-x}. The H_2 generation of TiO_2–N as high as ~200 μmol h^{-1} g^{-1} is much higher than that of TiO_{2-x} (115 μmol h^{-1} g^{-1}), even superior to previously reported doped TiO_2 (<150 μmol h^{-1} g^{-1}).[17,49,52,53] The larger amount of H_2 produced by the TiO_2–N is mainly due to its larger visible-light absorption than the other TiO_2–X. The obvious improvement of H_2 generation amount of these black titania under either full sun light or visible-light irradiation confirms the statement of reducing recombination centers by X incorporation discussed above.

The photocatalytic activities for the TiO_2–X samples were further evaluated by monitoring the decomposition of methyl orange (MO) in an aqueous solution under visible light and UV light irradiation, respectively. As shown in Fig. 4c, all of the

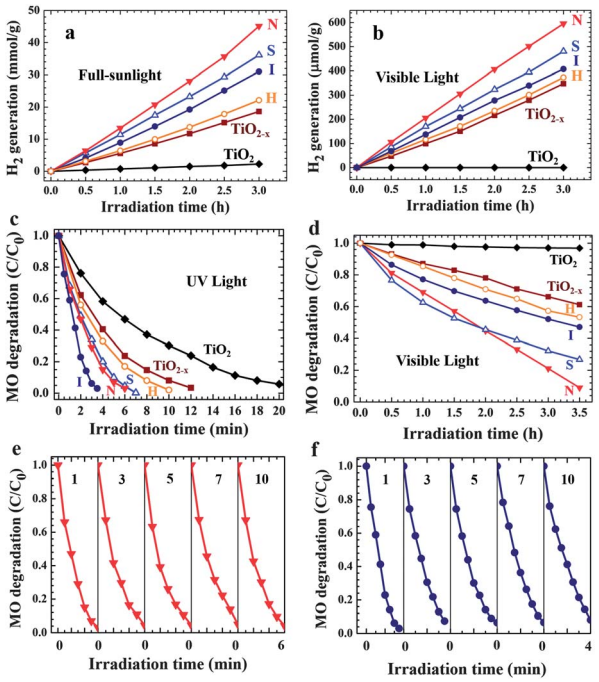

Fig. 4 Evaluation of the photocatalytic activities of TiO_2–X (X = H, N, S, I). (a) Full-sunlight and (b) visible-light driven photocatalysis for H_2 generation; (c) UV-light driven photocatalytic decomposition of MO over TiO_2–X. (d) Visible-light decomposition of MO over TiO_2–X. (e and f) Cycling tests of UV light irradiation photocatalytic activities (MO decomposition) of the TiO_2–N (e) and TiO_2–I nanocrystals (f).

TiO_2–X samples possess better photocatalytic activity than TiO_{2-x} driven by UV light. Surprisingly, the photocatalytic activity of TiO_2–I almost completely degraded MO only in 4 min. The time for almost complete degradation of MO UV-degradation in order is TiO_2–I (4 min) < TiO_2–N (6 min) < TiO_2–S (7 min) < TiO_2–H (10 min) < TiO_{2-x} (12 min) < P25 (20 min). The X incorporation in TiO_{2-x} is very effective in improving the UV photocatalysis. Furthermore, the TiO_2–N and TiO_2–I nanocrystals retained excellent photocatalytic activities in ten cycles shown in Fig. 4(e and f). It is more important to evaluate the visible-light decomposition, since the reported black TiO_{2-x} samples have a rather poor ability for visible-light photocatalysis.[14] Shown in Fig. 4d, the X (H, N, S, I) incorporation in TiO_{2-x} greatly improved the visible-light photocatalysis. TiO_2–N almost completely decomposed the organic contaminant in 3.5 h, compared with the ~60% residual MO for TiO_{2-x}. The residual MO after the 3.5 h degradation in order are TiO_2–N (0) < TiO_2–S (26.8%) < TiO_2–I (47.1%) < TiO_2–H (53.3%) < TiO_{2-x} (61.2%). The mineralization of MO is due to the oxidization of the holes from the photocatalyst.[54,55] The charge transfer between TiO_2–I and MO is much easier than between TiO_2–N and MO. It is understandable that the energy-level matching between TiO_2–I and MO is appreciable in promoting the oxidization reaction of MO.[56] Furthermore, the polarization ability of I is larger than that of N. This is why TiO_2–I has a better MO-degradation ability than TiO_2–N under UV-light irradiation.

Compared with the I-, N- and S-doped TiO_2 samples which followed literature preparations, our TiO_2–X samples possess higher doping levels, larger visible light absorption and much better photocatalytic activity not only under UV light but also under visible light, as shown in Fig. S14–17.† Since the traditional I-, N- and S-doped TiO_2 have no similar core–shell structure to our titania, the amorphous shell and the X termination for black titania may be necessary for ensuring their good photocatalysis.

Despite enhanced solar absorption, the black TiO_{2-x} displays insufficient photocatalytic activity under visible-light irradiation, similar to the reported black titania.[18] The black coloration relies on the transitions between the deeply localized Ti^{3+} $3d^1$ electrons and the unoccupied Ti 3d states and between the O^{2-} $2p^6$ at the valence band maximum and the unoccupied Ti 3d states. Enhanced wide-spectrum light absorption of the TiO_{2-x} can produce extra light-excited electrons and holes and cause better UV light photocatalytic activity than pristine TiO_2, but its visible-light photocatalysis was still poor. The trapped states from oxygen vacancies may be closely related to visible light absorption and photocatalysis. The doped X (H, N, S, I) atoms in TiO_{2-x} can reduce the recombination of electrons and holes and further increase effective light absorption. Therefore, the visible-light photocatalysis of TiO_2–X was improved.

Conclusions

In summary, a novel two-step approach was utilized to prepare heavily nonmetal incorporated black titania. The oxygen-deficient TiO_{2-x} nanocrystals consisting of a unique core–shell structure of TiO_2@TiO_{2-x} were formed by using aluminum

Table 1 Photocatalysis of various titania as comparison

	Full-sunlight driven	Visible-light driven		UV-light driven
Sample	H_2 generation (mmol h^{-1} g^{-1})	H_2 generation (μmol h^{-1} g^{-1})	Degradation time (h)	Degradation time (min)
TiO_2 (P25)	0.75	0	—	20
TiO_{2-x}	6.2	115	7.5	12
TiO_2-H	7.4	123	7.0	10
TiO_2-N	15.0	200	3.5	6
TiO_2-S	12.1	135	5.0	7
TiO_2-I	10.3	160	6.0	4
Literature	~10 (ref. 49–51)	~150 (ref. 49 and 52)	—	—

reduction in an evacuated two-zone furnace. The oxygen-deficient amorphous shells are responsible for the wide-spectrum light absorption and high nonmetal doping level of X (X = H, N, S, I). Such TiO_2–X samples gain enhanced photocatalytic activity not only under the irradiation of full-sunlight but also under visible light. Complete MO degradation for TiO_2–I took less than 4 min for UV light, and the H_2 generation of TiO_2–N is as high as 15.0 mmol h^{-1} g^{-1} under full-sunlight irradiation and 200 μmol h^{-1} g^{-1} for visible-light, superior to the ever-reported titania photocatalysts. The excellent photocatalysis of TiO_2–X is attributed to solar absorption enhancement and recombination center reduction. These outstanding improvements are attributed to the core–shell structure and unique electronic structure by band engineering of the Ti 3d states and the X valence states.

Experimental section

Preparation of black TiO_{2-x}

The synthesis of TiO_{2-x} is described in detail in our previous work.[10,24,28] Briefly, the P25 powders (0.5 g) were separately placed in a two-zone evacuated furnace (see Fig. S2a†) and treated at 500 °C for 6 h, where aluminum powders were put in the zone setting at 800 °C. The pressure in the furnace is 0.5 Pa.

Preparation of H-doped black titania (TiO_2–H)

The hydrogenation of TiO_{2-x} was performed in a thermal plasma furnace by hydrogen plasma for 4 h at 500 °C, as shown in Fig. S2b.† The plasma input power was 200 W.

Preparation of S- and I-doped black titania (TiO_2–S, I)

The TiO_2–S and TiO_2–I were prepared by the reaction of the as-prepared TiO_{2-x} with S and I_2 atmosphere at 500 °C for 4 h, respectively, as shown in Fig. S2c.† The resultant products were dispersed in CS_2 (ethanol for I_2) solution under stirring to remove residual S (I_2) to obtain TiO_2–S (TiO_2–I) samples.

Preparation of N-doped black titania (TiO_2–N)

The black TiO_{2-x} powder was treated at 500 °C for 4 h under a NH_3 : Ar = 2 : 1 gas flow at atmospheric pressure, as shown in Fig. S2d.†

Photocatalytic H_2 generation

Hydrogen production by photocatalytic H_2 generation was carried out in a top-irradiation Pyrex reaction cell as shown in Fig. S12.† 100 mg photocatalyst powder was dispersed by ultrasonication in a 200 mL aqueous solution containing 40 mL methanol as the sacrificial reagent. 0.5 wt% Pt was loaded *in situ* by impregnation 0.05 mL of H_2PtCl_6 (10 g L^{-1}) in the suspension. A Xe lamp (300 W) with 100 mW cm^{-2} was used for full-sunlight-driven photocatalytic H_2 generation. For visible-light driven photocatalytic H_2 generation, a Xe lamp (300 W) with a 400 nm cut-off filter (90 mW cm^{-2}) was used to cut off the UV light and allow only visible light to pass through. This filter can cut off >99.9% UV light, confirmed by the UV-vis absorption spectrum in Fig. S13.† The temperature of the reaction solution was maintained at room temperature by a flow of water. The evolved H_2 amount was determined using a gas chromatograph (Shanghai, GC-7900, TCD, N_2 carrier).

Photocatalytic methyl orange degradation

The photocatalytic activity was evaluated by the decomposition of methyl orange (MO) in a deionized water solution with an initial concentration of 20 mg L^{-1}. A total of 0.1 g of catalyst was added to 100 mL of MO solution. For UV-light photocatalysis, a 250 W mercury lamp was used as a light source for photocatalytic reaction. For visible light MO degradation, a 300 W Xe lamp with a 400 nm cut-off filter was used to cut off the UV light. The photodegradation of MO was observed by using absorption spectroscopy. At given time intervals, the solution was analyzed by recording variations of the absorption band maximum (460 nm) in the absorption spectra of MO.

In the durability test of TiO_{2-x} catalyst in the photodegradation of MO under UV light, ten consecutive cycles were tested. After each cycle, the catalyst was isolated by centrifugation and washed with water, and then fresh MO solution was added to the catalyst.

Sample characterizations

The samples were investigated with TEM (JEOL JEM 2100F) and XRD (Bruker D8 Avance). XPS experiments were carried out on a RBD upgraded PHI-5000C ESCA system (Perkin Elmer) with Mg Kα radiation ($h\nu$ = 1253.6 eV). The EPR spectra were collected using a Bruker EMX-8 spectrometer at 9.875 GHz at 300 K. The magnetic performance was conducted by a Physical Property Measurement System (Quantum Design Company).

Acknowledgements

T. Lin, C. Yang and Z. Wang contributed equally to this work. This work is financially supported by NSF of China (Grant no. 51125006, 91122034, 51121064, 61376056) and STC of Shanghai (no. 13JC1405700).

Notes and references

1 A. Fujishima and K. Honda, *Nature*, 1972, **238**, 37.
2 M. Lv, D. Zheng, M. Ye, J. Xiao, W. Guo, Y. Lai, L. Sun, C. Lin and J. Zuo, *Energy Environ. Sci.*, 2013, **6**, 1615.
3 Y. Li, H. Wang, Q. Feng, G. Zhou and Z. S. Wang, *Energy Environ. Sci.*, 2013, **6**, 2156.
4 R. Asahi, T. Morikawa, T. Ohwaki, K. Aoki and Y. Taga, *Science*, 2001, **293**, 269.
5 J. H. Park, S. Kim and A. J. Bard, *Nano Lett.*, 2005, **6**, 24.
6 X. Lü, X. Mou, J. Wu, D. Zhang, L. Zhang, F. Huang, F. Xu and S. Huang, *Adv. Funct. Mater.*, 2010, **20**, 509.
7 J. Wang, D. N. Tafen, J. P. Lewis, Z. Hong, A. Manivannan, M. Zhi, M. Li and N. Wu, *J. Am. Chem. Soc.*, 2009, **131**, 12290.
8 K. Xie, N. Umezawa, N. Zhang, P. Reunchan, Y. Zhang and J. Ye, *Energy Environ. Sci.*, 2011, **4**, 4211.
9 H. Tong, N. Umezawa and J. Ye, *Chem. Commun.*, 2011, **47**, 4219.

10 G. Zhu, T. Lin, X. Lu, W. Zhao, C. Yang, Z. Wang, H. Yin, Z. Liu, F. Huang and J. Lin, *J. Mater. Chem. A*, 2013, **1**, 9650.
11 C. Di Valentin, G. Pacchioni and A. Selloni, *J. Phys. Chem. C*, 2009, **113**, 20543.
12 C. Yang, Z. Wang, T. Lin, H. Yin, X. Lü, D. Wan, T. Xu, C. Zheng, J. Lin, F. Huang, X. Xie and M. Jiang, *J. Am. Chem. Soc.*, 2013, **135**, 17831.
13 G. Liu, L. C. Yin, J. Wang, P. Niu, C. Zhen, Y. Xie and H. M. Cheng, *Energy Environ. Sci.*, 2012, **5**, 9603.
14 X. Chen, L. Liu, P. Y. Yu and S. S. Mao, *Science*, 2011, **331**, 746.
15 F. Zuo, K. Bozhilov, R. J. Dillon, L. Wang, P. Smith, X. Zhao, C. Bardeen and P. Feng, *Angew. Chem., Int. Ed.*, 2012, **51**, 6223.
16 G. Wang, H. Wang, Y. Ling, Y. Tang, X. Yang, R. C. Fitzmorris, C. Wang, J. Z. Zhang and Y. Li, *Nano Lett.*, 2011, **11**, 3026.
17 X. Chen, L. Liu, Z. Liu, M. A. Marcus, W. C. Wang, N. A. Oyler, M. E. Grass, B. Mao, P. A. Glans, P. Y. Yu, J. Guo and S. S. Mao, *Sci. Rep.*, 2013, **3**, 1510.
18 Z. Wang, C. Yang, T. Lin, H. Yin, P. Chen, D. Wan, F. Xu, F. Huang, J. Lin, X. Xie and M. Jiang, *Adv. Funct. Mater.*, 2013, **23**, 5444.
19 Z. Zheng, B. Huang, X. Meng, J. Wang, S. Wang, Z. Lou, Z. Wang, X. Qin, X. Zhang and Y. Dai, *Chem. Commun.*, 2013, **49**, 868.
20 X. Liu, H. Xu, L. R. Grabstanowicz, S. Gao, Z. Lou, W. Wang, B. huang, Y. Dai and T. Xu, *Catal. Today*, 2013, DOI: 10.1016/j.cattod.2013.08.025.
21 S. Hoang, S. P. Berglund, N. T. Hahn, A. J. Bard and C. B. Mullins, *J. Am. Chem. Soc.*, 2012, **134**, 3659.
22 C. Sun, Y. Jia, X. H. Yang, H. G. Yang, X. Yao, G. Q. Lu, A. Selloni and S. C. Smith, *J. Phys. Chem. C*, 2011, **115**, 25590.
23 T. Xia and X. Chen, *J. Mater. Chem. A*, 2013, **1**, 2983.
24 H. Yin, T. Lin, C. Yang, Z. Wang, G. Zhu, T. Xu, X. Xie, F. Huang and M. Jiang, *Chem.–Eur. J.*, 2013, **19**, 13313.
25 X. Jiang, Y. Zhang, J. Jiang, Y. Rong, Y. Wang, Y. Wu and C. Pan, *J. Phys. Chem. C*, 2012, **116**, 22619.
26 A. Naldoni, M. Allieta, S. Santangelo, M. Marelli, F. Fabbri, S. Cappelli, C. L. Bianchi, R. Psaro and V. Dal Santo, *J. Am. Chem. Soc.*, 2012, **134**, 7600.
27 Z. Zheng, B. Huang, J. Lu, Z. Wang, X. Qin, X. Zhang, Y. Dai and M. H. Whangbo, *Chem. Commun.*, 2012, **48**, 5733.
28 Z. Wang, C. Yang, T. Lin, H. Yin, P. Chen, D. Wan, F. Xu, F. Huang, J. Lin, X. Xie and M. Jiang, *Energy Environ. Sci.*, 2013, **6**, 3007.
29 S. M. Prokes, J. L. Gole, X. Chen, C. Burda and W. E. Carlos, *Adv. Funct. Mater.*, 2005, **15**, 161.
30 M. A. Henderson, W. S. Epling, C. H. F. Peden and C. L. Perkins, *J. Phys. Chem. B*, 2003, **107**, 534.
31 E. Finazzi, C. Di Valentin, G. Pacchioni and A. Selloni, *J. Chem. Phys.*, 2008, **129**, 154113.
32 R. L. Kurtz, R. Stock-Bauer, T. E. Msdey, E. Román and J. De Segovia, *Surf. Sci.*, 1989, **218**, 178.
33 H. Li, X. Zhang, Y. Huo and J. Zhu, *Environ. Sci. Technol.*, 2007, **41**, 4410.
34 S. Badrinarayanan, S. Sinha and A. B. Mandale, *J. Electron Spectrosc. Relat. Phenom.*, 1989, **49**, 303.
35 M. V. Kuznetsov, J. F. Zhuravlev and V. A. Gubanov, *J. Electron Spectrosc. Relat. Phenom.*, 1992, **58**, 169.
36 J. F. Marco, J. R. Gancedo, M. A. Auger, O. Sánchez and J. M. Albella, *Surf. Interface Anal.*, 2005, **37**, 1082.
37 P. Padmavathy, R. Ananthakumar, B. Subramanian, C. Ravidhas and M. Jayachandran, *J. Appl. Electrochem.*, 2011, **41**, 751.
38 T. Umebayashi, T. Yamaki, S. Yamamoto, A. Miyashita, S. Tanaka, T. Sumita and K. Asai, *J. Appl. Phys.*, 2003, **93**, 5156.
39 X. Tang and D. Li, *J. Phys. Chem. C*, 2008, **112**, 5405.
40 W. E. Morgan, J. R. Van Wazer and W. J. Stec, *J. Am. Chem. Soc.*, 1973, **95**, 751.
41 S. Tojo, T. Tachikawa, M. Fujitsuka and T. Majima, *J. Phys. Chem. C*, 2008, **112**, 14948.
42 W. Su, Y. Zhang, Z. Li, L. Wu, X. Wang, J. Li and X. Fu, *Langmuir*, 2008, **24**, 3422.
43 S. V. Chong, K. Kadowaki, J. Xia and H. Idriss, *Appl. Phys. Lett.*, 2008, **92**, 232502.
44 P. F. Chester, *J. Appl. Phys.*, 1961, **32**, 2233.
45 G. Barolo, S. Livraghi, M. Chiesa, M. C. Paganini and E. Giamello, *J. Phys. Chem. C*, 2012, **116**, 20887.
46 C. Di Valentin, G. Pacchioni, A. Selloni, S. Livraghi and E. Giamello, *J. Phys. Chem. B*, 2005, **109**, 11414.
47 J. C. Yu, J. G. Yu, W. K. Ho, Z. T. Jiang and L. Z. Zhang, *Chem. Mater.*, 2002, **14**, 3808.
48 Q. Xiang, K. Lv and J. Yu, *Appl. Catal., B*, 2010, **96**, 557.
49 X. Chen, S. Shen, L. Guo and S. S. Mao, *Chem. Rev.*, 2010, **110**, 6503.
50 S. R. Chen, Y. P. Zhai, G. L. Xu, Y. X. Jiang, D. Y. Zhao, J. T. Li, L. Huang and S. G. Sun, *Electrochim. Acta*, 2011, **56**, 9549.
51 M. Zalas and M. Laniecki, *Sol. Energy Mater. Sol. Cells*, 2005, **89**, 287.
52 W. Xiao, J. Yuan, Y. Zhang and W. Shangguan, *Mater. Chem. Phys.*, 2007, **105**, 6.
53 H. B. Wu, H. H. Hng and X. W. Lou, *Adv. Mater.*, 2012, **24**, 2567.
54 A. L. Linsebigler, G. Lu and J. T. Yates, *Chem. Rev.*, 1995, **95**, 735.
55 M. R. Hoffmann, S. T. Martin, W. Choi and D. W. Bahnemann, *Chem. Rev.*, 1995, **95**, 69.
56 G. Liu, C. Sun, X. Yan, L. Cheng, Z. Chen, X. Wang, L. Wang, S. C. Smith, G. Q. Lu and H. M. Cheng, *J. Mater. Chem.*, 2009, **19**, 2822.

